# Review of Thermal and Electrical Modelling and Validation Approaches for Anode Design in Aluminium Reduction Cells

**Alexander Arkhipov[1], Nadia Ahli[2], Ievgen Necheporenko[3], Alexander Mukhanov[4], Lalit Mishra[5] and Vinko Potocnik[6]**

1. Manager - Modelling
2. Manager – Technology Transfer Contracts
3. Engineer II – R&D
4. Engineer I – R&D
5. Lead Engineer – R&D
6. Consultant

Emirates |Global Aluminium (EGA), Jebel Ali, Dubai, United Arab Emirates
Corresponding author:aarkhipov@ega.ae

**Abstract**

Anode assembly design has great impact on cell voltage and heat loss; therefore, it is one of the key elements of aluminium reduction cell design. Accurate measurements of anode voltage drops and heat loss on operating cells are difficult as they depend on anode age and anode cover. Mathematical modelling appears to be an easier way to take into account complex geometry and time dependence, but different modelling approaches still give significantly different results and conclusions on total anode assembly voltage drop as well as on different anode voltage components, heat loss and the potential for optimization. This paper discusses different aspects of anode assembly evaluation, such as thermo-electrical modelling and measurements for model and design validation. Special attention is given to anode stub-to-carbon contact resistance and anode-to-bath interface modelling.

## 1. Introduction

Anode assembly design has great impact on cell voltage and heat loss and therefore, it is one of the key elements of aluminium reduction cell design. The aluminium reduction cell loses up to 50 % of heat from the top while the anode voltage drop (AVD) contributes approximately 10 % to net cell voltage. Today, many smelters are focusing on increasing amperage and/or reduction of specific energy consumption which requires an accurate knowledge of the anode assembly heat loss and anode voltage drop in order to calculate them with adequate accuracy to support the design or operational parameters change.

Obtaining accurate measurements of anode voltage drops and heat loss on operating cells are difficult as they depend on anode age and anode cover thickness and composition. Another factor which makes it difficult to measure the required parameters precisely is harsh conditions in and around the cells as well as safety rules.

There are different approaches for modelling cell electric and heat balance. Some of them consider anodes and cathodes together with molten bath and metal in one model [1-3], others consider anode and cathode models separately or together but exclude liquid bath and metal from the model [4-6] and represent heat transfer from molten layers to cathode and anode by heat transfer coefficients. Some authors include only bath for anode modelling [7-9].

From heat transfer point of view, we suppose that all methods can give adequate results with proper validation of the model. But for electrical calculations in the anodes, inclusion of the bath and to a lesser extent the metal is obviously required because the bath has much higher electrical resistivity than the anode. Moreover, there is a bubble layer below the anode and back EMF on the bottom surface of the anode.

The bubble layer creates additional resistance in the bath which depends on the fraction of anode bottom covered by the bubbles; this resistance is not present on the anode sides, because the bubbles travel up the anode sides mostly detached from the anode surface. The bubble layer is assumed to be 5 mm thick, covering 50 % of anode bottom surface. To compensate, this is simulated by increasing the bath resistivity by a factor of 2 two in the bubble layer.

For anode modelling we consider only anodic part of back EMF, excluding cathode overvoltage, about 0.04 V, which is on the top of the metal pad away from the anode. Back EMF changes very little with current since it is proportional to the logarithm of the current. It can be linearized in the neighborhood of the current operating point and separated into a constant part, equal to the value at zero current, also called extrapolated voltage [10], and into the part proportional to the current, which we interpret as the resistive part. This is shown in Figure 1, where the back EMF is calculated from formulas in [10]. The constant part in the case shown is 1.65 V and the resistive part is equal to 0.150 V to make 1.80 V for the cell effective operating current density, which accounts for anode fanning (i.e., that some current flows out of the anode on the sides in the bath immersion). The resistive part of anodic back EMF is included in the model as contact resistance on anode bottom and sides, such that the resistive voltage drop across bath-anode interface is 0.150 V.

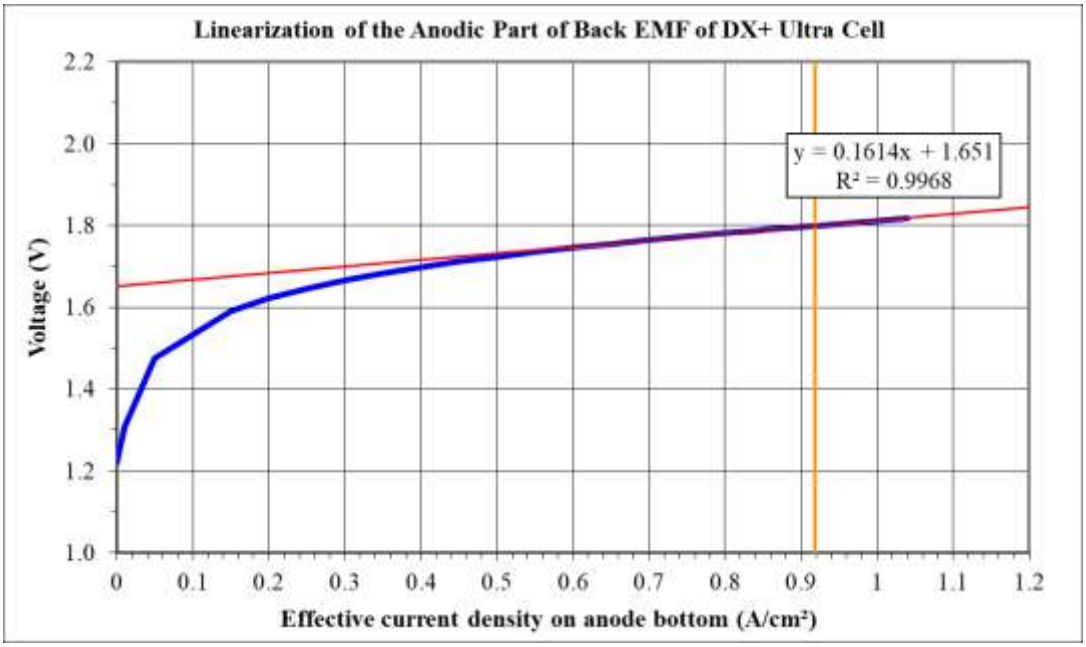


**Figure 1. Linearization (red) of the anodic part of back EMF (blue) in the neighbourhood of the cell operating point (yellow).**

To clarify these questions the ANSYS Mechanical 19.1 commercial finite element software package was used for modelling where several cases are explained below to establish the best method for the future consisting of omitting or including bath and metal, the bubble layer and the resistive part of anodic back EMF.

Voltage drop and anode current distribution depend on anode age since the anodes are consumed and there is less and less carbon below the stubs. The temperature in the upper part of the anode increases with time and in the stub area as well; thus increasing the pressure in the stub-cast-iron-carbon contact area while decreasing the contact resistance. Out of the cases studied in steady state, the best model was chosen to also calculate the voltage drops for different anode ages and the results are compared with measurements.

Impact of symmetry on AVD was checked because with amperage increase in the smelters the anode length is increased as much as possible to decrease the impact of amperage increase on anode-cathode distance (ACD), MHD stability and heat balance of the cell. Increasing the length towards the central

channel is limited by breaker diameter and the volume of bath required for alumina dissolution. As a result, the anode length is increased towards the side channel and the anode block becomes asymmetric with respect to the anode rod.

Another tendency in recent years has been introduction of slotted anodes. Today with slot height reaching up to 60 % of anode height or more, it is necessary to check the effect of slots on both the anode and bath voltage drop. On the other hand, the changes of the bubble layer coverage due to slots were not modeled, because this would require a much more complex model. We consider that the anode coverage by bubbles of 50 % of anode bottom is already representative for the bubble layer of slotted anodes.

Another study was carried out to check the impact of electrical transition joint (ETJ) on AVD.

## 2. Measurements

At EGA, the standard practice for anode voltage drop measurement is from anode rod under the anode beam to the anode underside (bottom face). A special hook with sharp tip, shown in Figure 2, is used for hooking the anode on the bottom surface. As standard practice, all anodes in a cell are measured, except the newly changed anode less than one day old. Several measuring rods are used as only a cold rod gives reliable result. Moreover, the best way to obtain good data is to use a cold rod for each measurement.

To make the measurement, the side channel crust is broken in the corner between two anodes. The hole has to be big enough to allow quick immersion of the hook into the bath and hooking the anode bottom with force to create good contact between rod tip and the anode carbon. The voltage reading may fluctuate sometimes but the minimum reading is recorded as we believe that it corresponds to the best contact and reflects more accurately real voltage drop.

Based on typical hook horizontal length and the assumption that the rod is always directed at 45 degrees from anode sides, the distance from anode corner to the location of measurement was calculated to be X = 84 mm and Y = 84 mm from the corner. The AVD is the measured difference of potentials between the anode rod under the beam and this point. In the models, the potential will also be determined at the same point and will be referred to as “AVD at measurement point”.

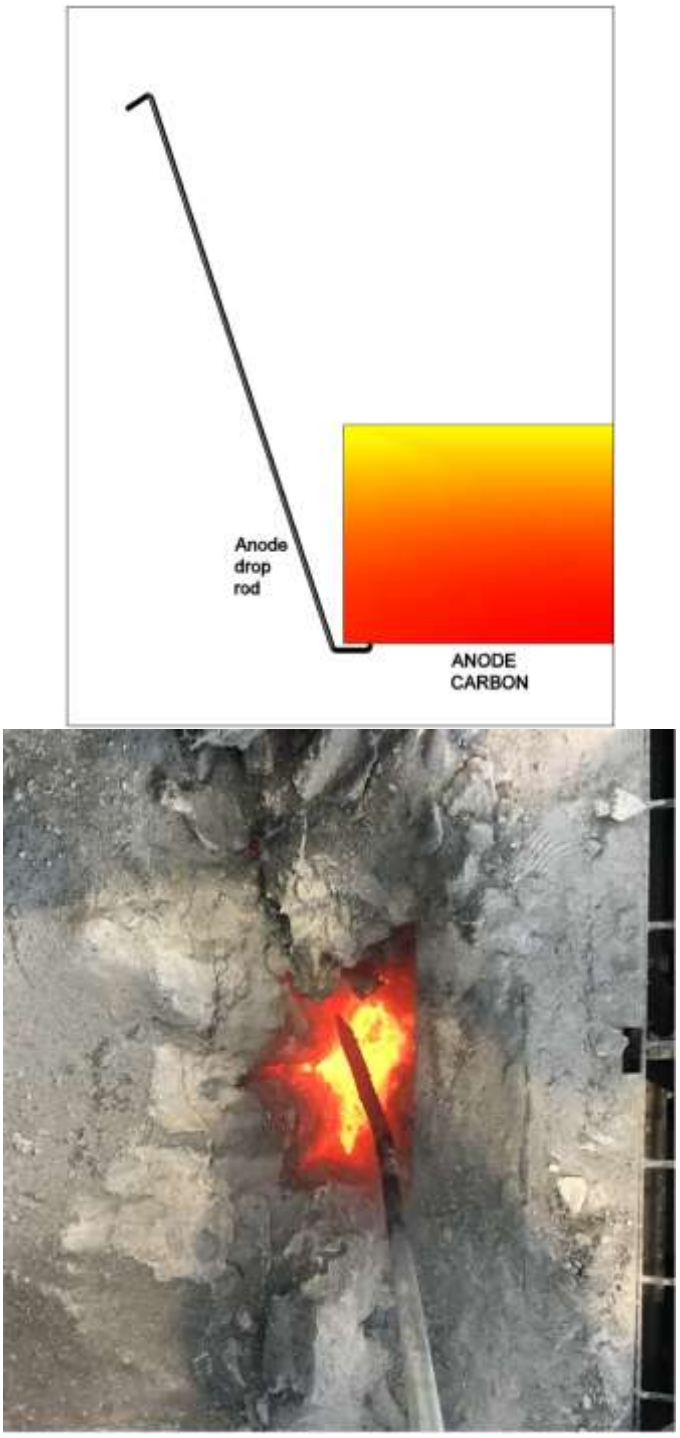


**Figure 2. Electrode for anode voltage drop measurements.**

To validate the thermal field, two types of measurements can be done: heat flux through the top of anode cover and temperatures on the top of anode cover, on the yoke and on the anode rod (Figure 3). Only the temperatures were measured. The yoke temperature was measured by infrared gun, but the anode rod temperature was measured by contact thermocouple because the emissivity of aluminium can vary in wide rage and infrared gun reading is not very accurate. The anode cover top temperature was measured by infrared gun on small steel plates put on the top surface one day in advance.

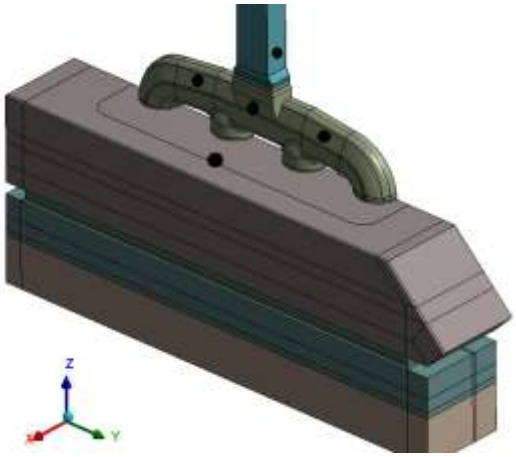


**Figure 3. Locations of temperature measurements (black spots) for thermal validation of anode model.**

## 3. Boundary Conditions and Modelling Approach

Anode assembly model geometry includes anode rod, ETJ, steel yoke and stubs, cast iron (CI), anode carbon block with 50 mm radius rounded edges at the bottom, liquid bath with 5 mm thick bubble layer and liquid metal (except in one case) as well as anode cover (Figure 4). The anode part of back EMF was represented by a contact resistance on the anode.

The model was meshed by hexa-mesh except the yoke which was meshed by tetra elements. Total number of nodes was about 205 000 and the number of elements 60 000. High order (quadratic) elements were used even though this is not required because of large number of elements, but this is the only option in ANSYS Workbench 19.1 for thermo-electric simulations.

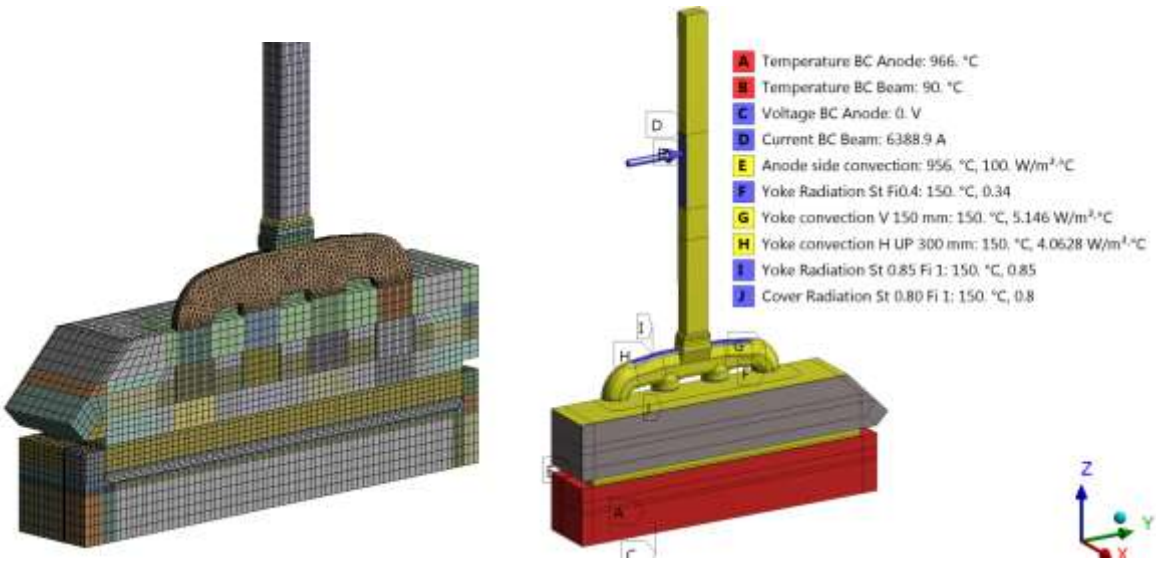


**Figure 4. Mesh (left) and boundary conditions (right) in the model. Model symmetry is assumed on the longitudinal axis of the anode as shown.**

In all models anode assembly material properties (thermal conductivity and electrical resistivity) were functions of temperature, except for titanium for which we have only room temperature data. Bath and liquid metal properties were constant due to boundary condition described below. Bubble layer resistivity was set to twice that of bath, with the assumption that this corresponds to 50 % of coverage of the anode bottom by bubbles.

The following boundary conditions were used:

1) Symmetry plane boundary condition (at anode longitudinal axis and at the middle of the centre channel) is zero normal current flow and zero normal heat flux (automatically assumed in ANSYS);
2) One half of anode current was applied to (one half) of the anode rod on contact with the anode beam, corresponding to cell current of 460 kA in DX+ Ultra cells;
3) For all models except the case without bath and metal, 0 V was applied to the bottom of the metal pad. Due to very low electrical resistivity of liquid aluminium compared to bath, it does not matter where exactly the 0 potential is applied in the metal because this will not affect current distribution in the bath and above. For the model without bath and metal, 0 V was applied to full anode bottom including the rounded part;
4) Temperature of 966 °C was fixed in full bath and metal volume therefore constant properties were applied;
5) Temperature of 90 °C was applied to contact area of the rod with the anode beam.
6) Heat transfer coefficient (HTC) of 100 $W/m^2K$ with ambient temperature ($T_{amb}$) of 956 °C was applied to anode sides in the space between the bath and the crust (which was 50 mm above the bath) to take into account convection and radiation from hot bath;
7) Convective heat transfer coefficients were calculated and applied to external surfaces of the yoke, ETJ, rod and cover as function of temperature based on empirical equations using special ANSYS Parametric Design Language (APDL) macro taking into account surface orientation, size, surface and ambient temperature ($T_{amb}$) which was 150 °C for surfaces inside the hood and 40 °C for the rod outside the hood.
8) Radiation boundary conditions were applied to the same surfaces. For each surface, the emissivity was multiplied by view factor and the radiation reference temperature $T_0$ was the same as ambient temperature for convection. Some heat from the yokes is also transferred to the anode cover. View factors between different yoke surfaces and anode cover were calculated manually in a special Excel template. The assumption was made that all radiation heat transferred from the yoke to the anode cover stays in the system, therefore, it should not be counted in overall heat loss even if it changes slightly the yoke and the anode cover temperature locally. View factor for vertical faces of the yoke was set to 0.4, horizontal top surface to 1 and for the bottom horizontal surface, the radiation was not applied.

The modelling study was carried out to answer the questions raised above. The following cases were studied:

1) Base Case. Mid-life anode. Includes all parts mentioned above: anode rod, ETJ, yoke and stubs, CI, 400 mm high anode carbon block (mid-life anode), liquid bath, bubble layer and anode cover. Impact of liquid aluminium was checked separately:
    a. With liquid aluminium: 0 V applied to full bottom of metal.
    b. Without liquid aluminium: 0 V applied to full bottom of bath.
2) Base Case but without bath and metal. 0 V applied to anode bottom with rounded corners;
3) No bubbles. Base case but without bubble layer. Resistivity of this layer is that of bath.
4) Back EMF. Base case but electrical contact resistance applied at the interface between anode bottom and sides and bath to get extra 0.15 V total voltage drop.
5) Butt. The same as base case but anode carbon height reduced to 250 mm which corresponds to approximately 5-6 days before anode change.
6) New. The same as base case but anode carbon height increased to 550 mm.
7) Mid age with slots. Base case but two slots are added in the model. Slot height is 110 mm below the bottom of the stubs. Slot width is 10 mm.
8) New with two slots. The same as Case 6 but with two slots as in Case 7.

Using Base model the following cases were checked for the impact of electrical transition joint (ETJ) on AVD:

1) Base case without titanium layer. The weld of aluminium to ETJ is 30 mm wide, the weld of steel yoke to ETJ is 15 mm wide.
2) 1.5 mm of titanium added in the model.
3) Full contact between ETJ, rod and yoke.

4) Full contact between ETJ and rod only.

Also the top shape of the yoke in contact with ETJ is considered separately in two cases.

## 4. Modelling Results for the Base Case of DX+ Ultra Cell

First of all, the Base Case and Case 2 (no melt) models were calibrated by changing electric contact resistance (translated into ANSYS as contact conductivity) between CI and carbon to get the same calculated AVD at measurement point as measured AVD at anode mid-life.

As expected, models with and without liquid aluminium (Cases 1a and 1b) gave exactly same results (up to second digit after decimal point), therefore, Base Case is #1 in result tables without mentioning a or b.

The model for mid age anode without slots with bath and bubble layer was taken as the Base Case. The temperature field and voltage drop for full model are shown in Figure 5. In Table 1 typical heat loss distribution and in Table 2 heat inputs are shown. Electrical balance can be found in Table 3.

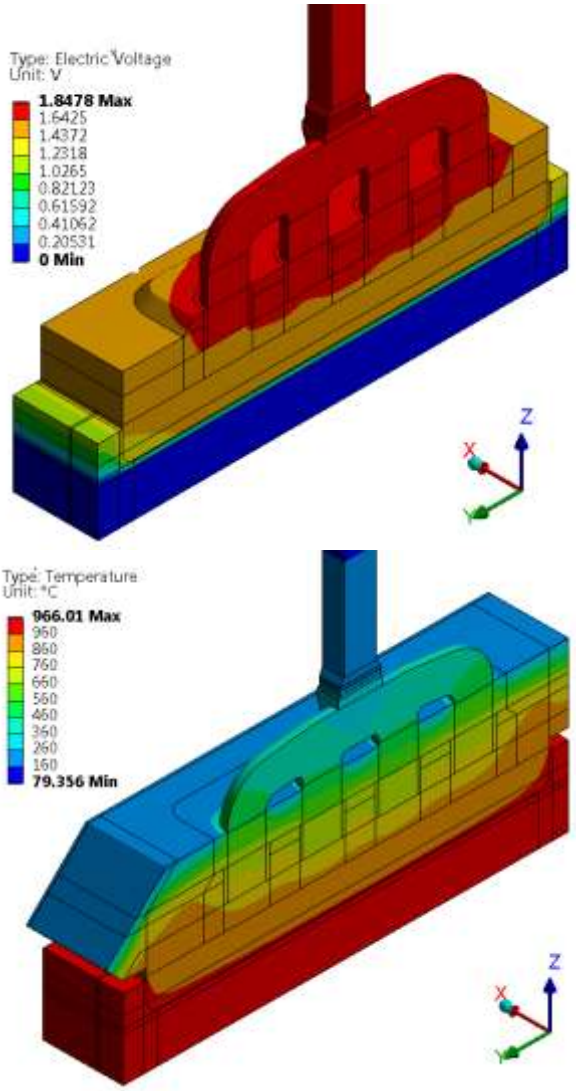


**Figure 5. Voltage and temperature field for Base Case.**

**Table 1. Heat loss distribution for Base Case.**

| Component | Heat loss, kW | Heat loss, % |
|---|---|---|
| Rod | 53.3 | 18.2 |
| Yoke | 138.9 | 47.4 |
| Cover | 101.0 | 34.5 |
| Total | 293.1 | 100.0 |

**Table 2. Heat input distribution for Base Case.**

| Component | Heat input, kW | Heat input, % |
|---|---|---|
| Bath to immersed anode | 108.0 | 36.8 |
| Bath to anode side and crust | 19.5 | 6.7 |
| Joule heat from anode voltage drop of 0.36 V | 165.6 | 56.5 |
| Total | 293.1 | 100.0 |

## 5. Comparison of Results for Different Modelling Approaches

To understand different results from different approaches, we analyzed electric potential distribution and current density at the anode bottom.

As it can be seen from Figure 6a, 7a, 8a and 9, the base case gives a high gradient of electrical potential on anode bottom but quite uniform current density up to the edges, where the current density has a spike. The increased current density at the edges is partially due to the assumption that the bubble layer ends where the anode curvature starts. However, increased current density is seen even in the case without bubbles (Case 3), which means that the anode should be more rounded than in the model, now. In fact, higher current density would consume the anode faster and round up the edges more. Case 2 with no melt and 0 electric potential on the bottom of the anode gives non-uniform current density at the bottom of the anode, shown in Figures 6b, 7b, 8b and 9. The voltage contours in Figure 6b are shown from a different angle because the bottom would be the same dark blue color if viewed from the bottom due to 0 V fixed on entire bottom. If Case 2 was a real situation, the anode consumption in the center would be much faster than closer to the edges and these would stay sharp not rounded as in reality.

The main negative consequence of modelling the anode without the melt is that contact voltage drop between cast iron of stubs and anode stub-hole carbon can be drastically overestimated. As it was described before, AVD is measured from anode rod below clamp to a point close to the corner from side channel. As we can see from modelling results in Table 3, the calculated voltage drop in that location (449 mV) is much higher than the average over the anode bottom (360 mV) for the Base Case with melt. But when 0 potential is applied to full anode bottom, the average anode assembly voltage drop equals to the one at measurement point. In order to match the measured AVD to the calculated one at the measurement point, the required contact voltage drop in Base Case is 22.5 mV and in Case 2 it has to be 106.4 mV. Overestimation of contact voltage drop, firstly, can give us impression that it is high and it can push us to make a lot of effort to reduce it. Secondly, for a given cell voltage the ACD would be by 2.3 mm greater in practice than calculated for an anode voltage drop overestimated by 90 mV.

AVD in Case 3 with no bubbles is by 1.3 mV lower than in the base case (Table 3).

Addition of contact resistance between bath and anode to represent 0.15 V of Back EMF increased AVD by 1 mV. Current fanning (Figure 8d) and bath voltage drop also slightly increased because the additional contact resistance at the bottom forced some more current through the sides of the anode into the channels.

Based on the results above we decided that Base Case approach will be used for all studies in the future.

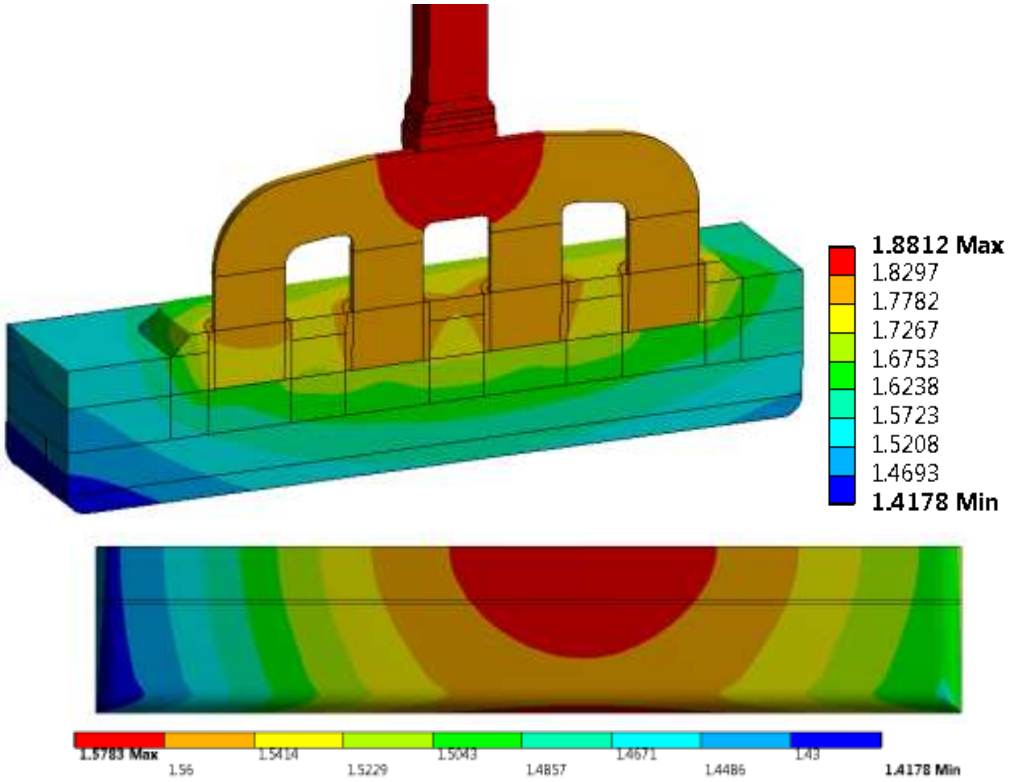


a) Base case

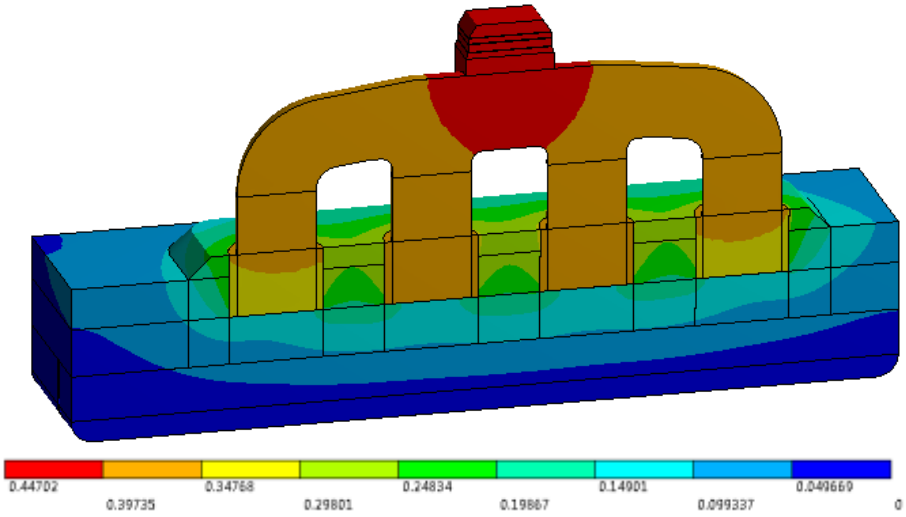


b) Without melt

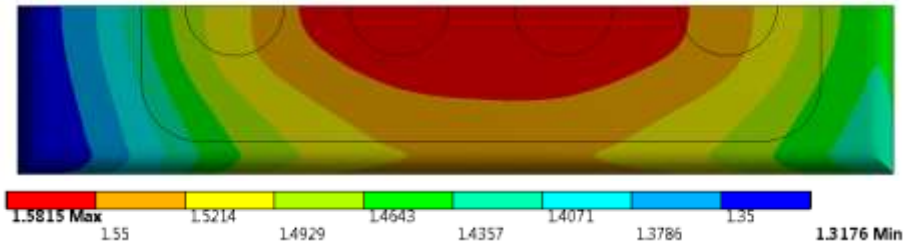


c) End of life

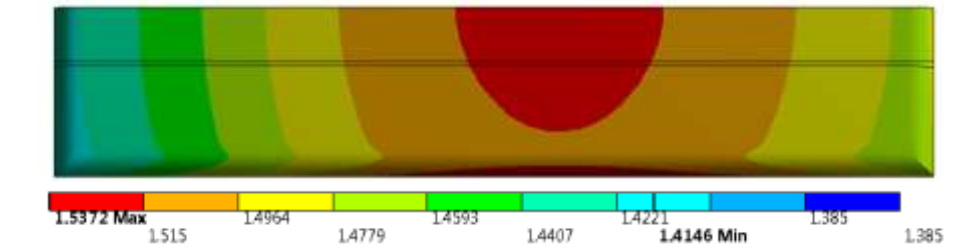


d) New anode

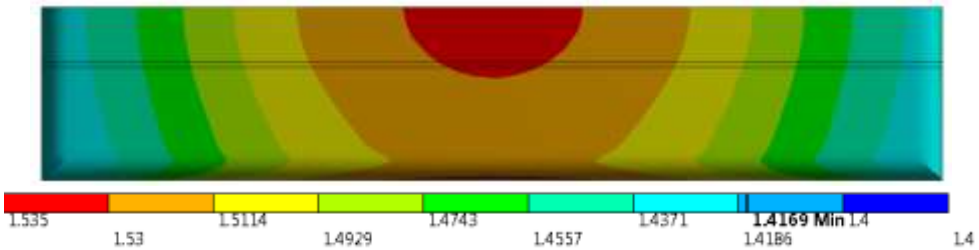


e) Symmetric anode

**Figure 6. Electrical potential. Side channel is on the left.**

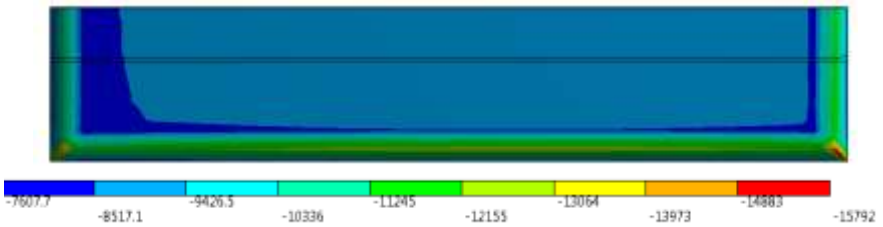


a) Base case

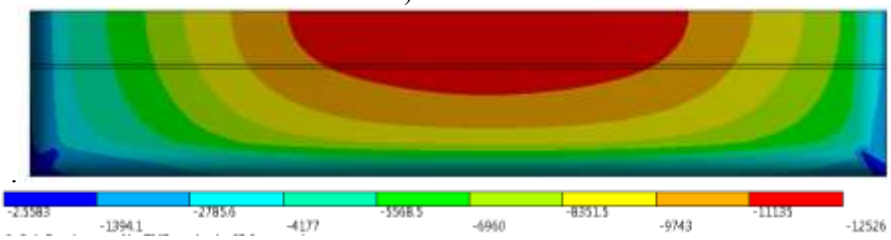


b) Without melt

**Figure 7. Vertical current density on anode bottom. Side channel is on the left.**

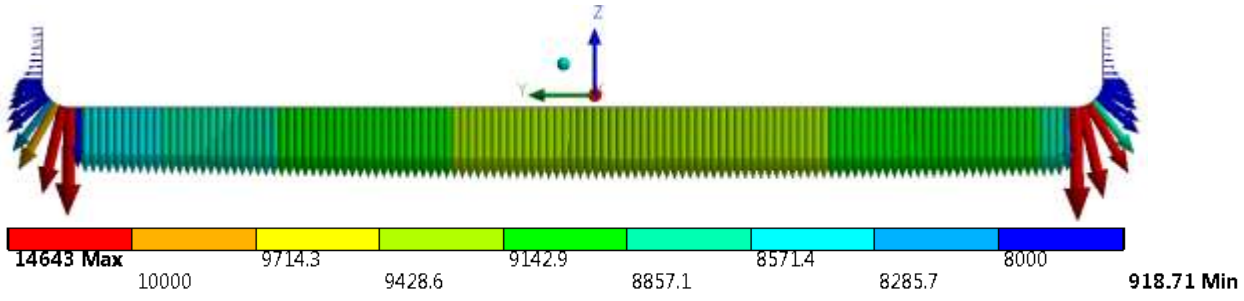


a) Base case

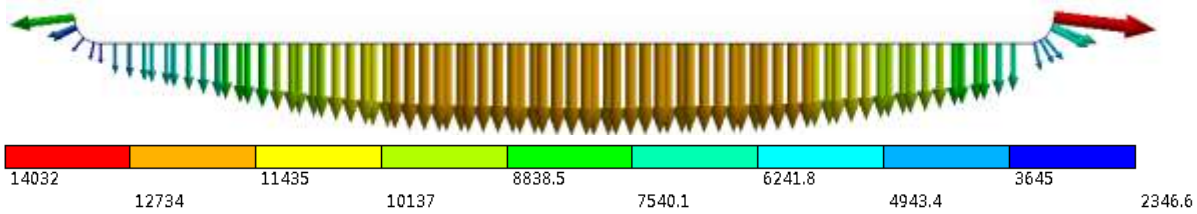


b) Without melt

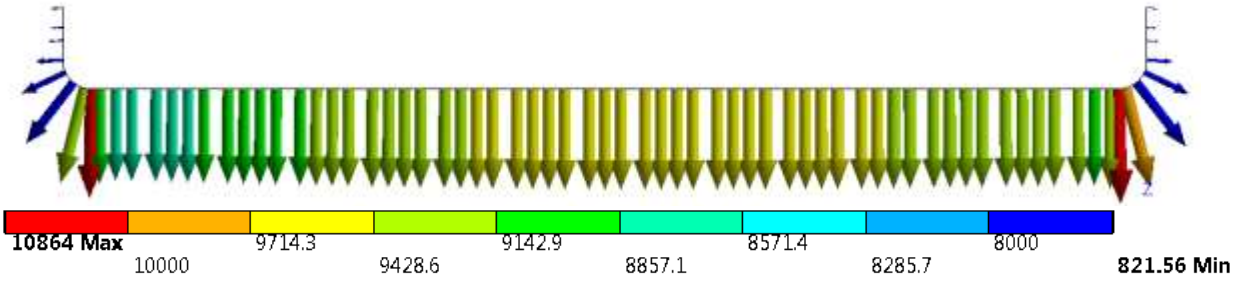


c) Without bubbles

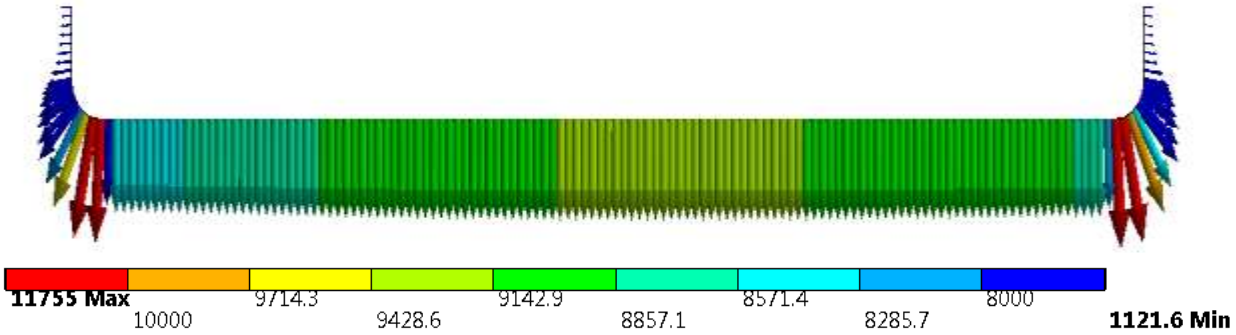


d) With Back EMF

**Figure 8. Current density on anode bottom at the middle (on symmetry plane). Side channel is on the left.**

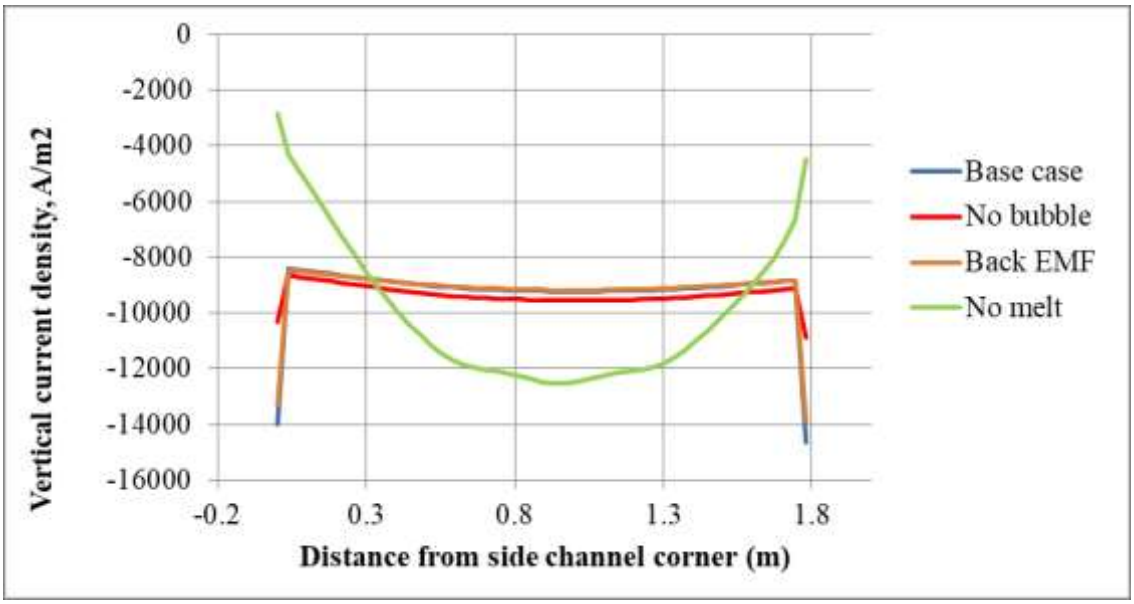


**Figure 9. Vertical current density leaving anode bottom, shown along the symmetry plane in the middle of the anode. Side channel is on the left. The curves are shown only on the flat bottom surface of the anode (rounded and vertical surfaces are excluded, because ANSYS takes only straight paths to plot variables).**

**Table 3. Thermo-electric results for different modelling approaches.**

| Case # | | 1 | 2 | 3 | 4 |
|---|---|---|---|---|---|
| | Unit | Base case | No melt | No bubbles | Back EMF |
| Anode voltage drop at measurement point | mV | **448.6** | **447.0** | **442.5** | **450.2** |
| Average Anode voltage drop | mV | **360.0** | **447.0** | **358.7** | **360.1** |
| Aluminium rod drop | mV | 17.8 | 17.9 | 17.8 | 17.8 |

| | | | | | |
|---|---|---|---|---|---|
| Transition joint | mV | 5.2 | 5.2 | 5.2 | 5.2 |
| Yoke | mV | 46.5 | 46.3 | 46.4 | 46.5 |
| Stubs | mV | 19.2 | 19.3 | 19.2 | 19.2 |
| Cast Iron | mV | 2.4 | 1.9 | 2.4 | 2.4 |
| CI contact to carbon | mV | 22.5 | 106.4 | 22.5 | 22.5 |
| Carbon block | mV | 246.6 | 250.1 | 245.3 | 246.6 |
| Bath | mV | 1487.3 | - | 1318.7 | 1488.8* |
| Metal | mV | 0.5 | - | 0.5 | 0.5 |
| **Delta AVD (At measurement point – Average on bottom)** | mV | **88.6** | **0.0** | **83.8** | **99.8** |
| **Heat loss** | kW | **293.1** | **309.2** | **-** | **293.6** |

*The resistive voltage drop of anode back EMF of 0.15 V is across the contact resistance on the anode surface.

Comparing the bath voltage drop between Case 1 with bubbles and Case 3 without bubbles, we see that the bubble voltage drop is only 169 mV instead of expected 206 mV from equations in [10] for 50 % coverage of anode surface by bubbles. To get 206 mV, higher resistivity than twice that of bath should be used; the right value in the model could be determined by trial and error. This means that the bubble voltage drop has more complex relationship to the bubble coverage of the anode than just proportional to the bath resistivity in the bubble layer used here.

Larger heat loss by 16 kW in case of higher anode voltage drop is less than half of 41 kW, generated in the anode by 89 mV larger voltage drop at 460 kA.

## 6. Impact of Anode Age on AVD

The modelling results in Table 4 and Figure 6 will be compared to the measured AVD shown in Figure 10.

The AVD in Figure 10 was measured from the top of anode rod below anode beam to the underside of the anode as described above. Four sets of measurements are from three cells at different times; each set consists of measuring all anodes in a cell, except those less than 2 days old and some for which the crust was too difficult to break. A few outliers were omitted. Altogether, 112 measurements are in the graphs. As a usual practice a linear trend with anode age is drawn and AVD at mid-age is calculated (Figure 10, top) and interpreted as “anode voltage drop”, which is 444 mV in this case. There is a clear decreasing trend with anode age; the difference between AVD at 2 days and 25 days is 107 mV. However, the comparison with the model will be more conclusive with Figure 10, bottom, which shows two separate trends: The largest decrease of 88 mV is in the first half of life and only a small decrease of 24 mV is in the second half.

Modelled average AVD for close to end-of-life age (25 cm anode height remaining, corresponding to the age of 23 days) decreased by 58 mV with respect to the mid-life but the difference between AVD at measurement point and average AVD increased by 67 mV from 89 mV to 156 mV (Table 4). The higher electrical potential gradient can be clearly seen in Figure 6c. This means that, according to the model, there should be no difference between the measured AVD at mid-life and end-of-life. This corresponds fairly well to what we see in Figure 10, bottom, where the measured decrease is only 24 mV, considering that modelling of an anode butt did not take into account the smaller anode bottom area and more rounded edges than in a new anode.

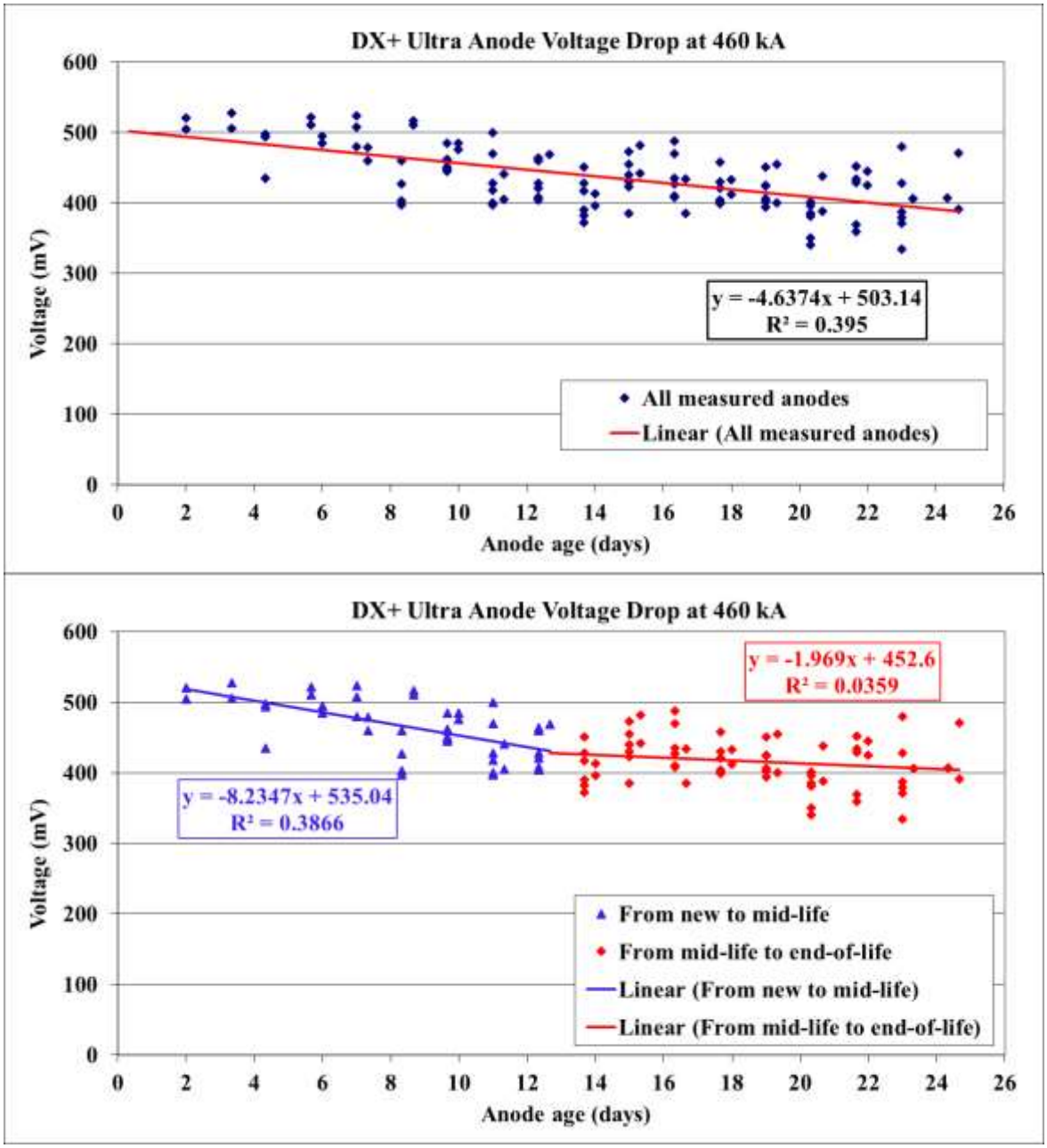


**Figure 10. AVD as a function of anode age for DX+ Ultra at 460 kA. Top: All data with linear trend. Bottom: The same data with two trends.**

AVD for relatively new anode (550 mm high, corresponding to the age of 23 days) increased by 61 mV but the difference between the calculated potential at measurement point and the average potential reduced to 0.2 mV (Table 4). This means that for young anodes, the measured value actually represents the modelled average value. On the other hand, the modelled value is lower than the measured one, which shows that the CI-to-carbon resistance in the model was not high enough for new anodes. The use of higher contact resistance for new anodes would be quite logical, since the stubs are colder in young anodes and there is less pressure between CI and carbon.

**Table 4.Thermo-electric results for different modelling approaches.**

| Case # | | 1 | 5 | 6 | 7 | 8 |
|---|---|---|---|---|---|---|
| | Unit | Base Case | Butt | New | Base& slots | New & slots |
| **Calculated anode voltage drop at measurement point** | mV | **448.6** | **458.4** | **421.4** | **454.7** | **428.9** |
| **Average Anode voltage drop** | mV | **360.0** | **302.5** | **421.2** | **366.3** | **428.5** |
| Aluminium rod drop | mV | 17.8 | 17.9 | 17.7 | 17.8 | 17.7 |
| Transition joint | mV | 5.2 | 5.0 | 5.0 | 5.2 | 5.0 |
| Yoke | mV | 46.5 | 48.9 | 45.2 | 47.2 | 45.7 |
| Stubs | mV | 19.2 | 20.6 | 18.4 | 19.8 | 18.7 |
| Cast Iron | mV | 2.4 | 2.4 | 2.3 | 2.5 | 2.4 |
| CI contact to carbon | mV | 22.5 | 20.8 | 22.5 | 22.3 | 22.3 |
| Carbon block | mV | 246.6 | 186.9 | 310.1 | 251.5 | 316.7 |
| Bath voltage drop | mV | 1487.3 | 1489.4 | 1486.8 | 1488.6 | 1488.2 |
| **Delta AVD (At measurement point – Average on bottom)** | mV | **88.6** | **155.9** | **0.2** | **88.4** | **0.4** |
| **Heat loss** | kW | **293.1** | **324.0** | **274.5** | **-** | **-** |

## 7. Impact of Anode Symmetry and Slots on Average AVD and Potential Gradient on Anode Bottom

Anode design change from symmetric to asymmetric has very small impact on average voltage drop (0.2 mV) but the asymmetry significantly increases the difference between calculated AVD at measurement point and average AVD, an increase of 30 mV (Table 4). Main reason for greater difference in asymmetric anodes is longer distance from outer stub to anode side at side channel; as consequence, the electric potential gradient between the point of measurement and the average increases.

Anode slots increase AVD by 6 mV at mid-age and by 7 mV for new anode (Table 4). This is much smaller than the contribution of slots to reduction of bubble voltage drop seems not high penalty.

**Table 5. Calculated voltage drops for different modelling approaches (mV).**

| Case | 1 | 2 | 3 | 4 |
|---|---|---|---|---|
| | Base Case | With Ti | Full ETJ Contacts | Full Al Contact |
| **Average Anode voltage drop** | **360.0** | **364.7** | **355.8** | **363.6** |
| Aluminium rod drop | 17.8 | 17.7 | 17.1 | 17.3 |
| Transition joint | 5.2 | 9.0 | 4.7 | 8.3 |
| Yoke | 46.5 | 47.3 | 43.3 | 47.3 |
| Stubs | 19.2 | 19.3 | 19.2 | 19.3 |
| Cast Iron | 2.4 | 2.4 | 2.4 | 2.4 |
| CI contact to carbon | 22.5 | 22.5 | 22.5 | 22.5 |
| Carbon block | 246.6 | 246.6 | 246.6 | 246.6 |

## 8. Electrical Transition Joint Voltage Drop

Results for different ETJ designs are shown in Tables 5 and 6. From the base case, ETJ voltage drop increases by 3 mV when 1.5 mm layer of titanium is added and it decreases by 4.3 mV in case of full electrical contact between the rod, yoke and ETJ, but it decreases only by 0.7 mV in case of full contact from aluminum side of ETJ to the rod. This means that a good width of weld between anode rod and ETJ is important only for mechanical strength and current overload in the anode. Any effort to reduce voltage drop in the ETJ welds needs to be focused on the steel part but there are some limitations:

- To increase horizontal welded area, the height of chamfer should also be increased, because to fill the weld properly 30-45 degree chamfer is required. The increase of chamfer height can lead to an increase of steel thickness of ETJ, which increases the voltage drop;
- A bigger weld joint could require much more time to weld because pauses are often required to avoid overheating of the tri-metallic connection.

Another important joint, which is sometimes not taken into account, is the top part of the yoke to which ETJ is welded. A decision for easier welding, taken without prior mathematical modelling, could lead to long term penalty. A reduction of cross-section (Figure 11) can lead to considerable increase in voltage drop, which has been demonstrated by modelling and proved in practice.

Table 6 shows the results of a study of the steel joint cross-section between ETJ and the top the yoke. A small discrepancy between modelled and measured voltage drops is due to omission of 1.5 mm thick titanium layer in the model. Otherwise, the modelled and measured a voltage drop agree well.

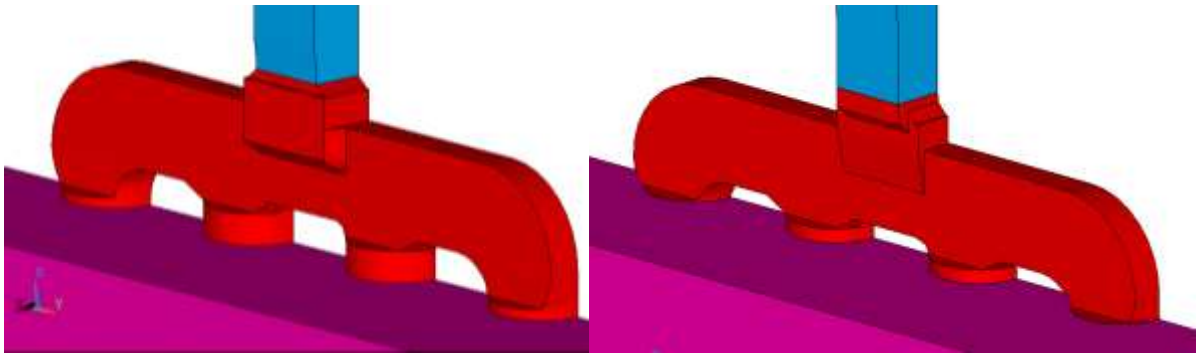

**Figure 11. Two yoke designs: Original with the same yoke upper part cross-section as ETJ (left) and with reduced cross-section of the upper part for easier and faster welding (right).**

**Table 6.Study of the steel joint cross-section between ETJ and the top of yoke.**

| | Unit | Original cross-section | Reduced cross-section | Difference |
|---|---|---|---|---|
| Measured joint voltage drop | mV | 10.5 | 19.1 | 8.6 |
| Modelled joint voltage drop | mV | 7.5 | 15.5 | 8 |
| Measured joint temperature | °C | 232 | 256 | 22 |
| Modelled joint temperature | °C | 225 | 247 | 25 |

## 9. Special Measurements to Check Uniformity of Electrical Potential at Anode Bottom

A special set of longer measuring rods was made to check potential gradients on the anode bottom. Measurements of anode voltage drop were made at different distances from anode edge during scheduled anode settings on anodes next to removed ones in two cells. Measured anodes had age 3 days on one side and 23 days on the other, which are pretty close to modelled 250 mm and 550 mm high anodes. Approximate distances along anode length for voltage drop measurements were 85 mm, 360 mm and 570 mm. Precise distance from anode side to measurement location was difficult to

measure due to safety issues with open cavity after anode removal.,) shown in Figure 12. Tables 7 and 8 show a comparison between measured and modeled values.

**Figure 12. Measurement of anode voltage drop in point 3.**

As we can see the difference between corner value and other points matches well between the model and the measurements for high age anode. The point at 570 mm is pretty far and according to technician making the measurement, the pressure which he could apply to the hook was much lower than for the point at 360 mm, so that the results are less for the distant point. For the relatively new anodes the difference between the measured and the modeled values is higher but the tendency is the same. For new anodes, the difference between points is much smaller in the model than in the measurement.

Quantitative difference between measured and modelled values for different ages can be due to the same contact resistance for new, mid-age and end-of-life anodes in the model.

**Table 7. Anode voltage drop for 23 days old anode.**

| Distance | 85 mm | 360 mm | 570 mm |
|---|---|---|---|
| 21 days, measured | 380 | 280 | 255 |
| Difference with corner | - | 100 | 126 |
| 21 days, ANSYS | 458 | 359 | 298 |
| Difference with corner | - | 99 | 160 |

**Table 8. Anode voltage drop for 3 days old anode.**

| Distance | 85 mm | 360 mm | 570 mm |
|---|---|---|---|
| 3 days, measured | 552.5 | 551.0 | 591.5 |
| Difference with corner | - | 1.5 | -39 |
| 3 days, ANSYS | 421 | 385 | 356 |
| Difference with corner | - | 36 | 65 |

## 10. Conclusions and Way Forward

Anode voltage drop model must have liquid bath because its high resistance determines entirely the electrical potential and current density distribution on the bottom of the anode. Bubble layer and back EMF are much less important to be included because they have much smaller resistance than the

whole bath; nevertheless, it is good to have them in the model as they do not bring additional complexity to the model or increase the solution time.

Measured anode voltage drop from the top of the anode rod to the point near the back-wall corner of the anode overestimates the average AVD to an increasing extent from younger to older anodes. Only for young anodes the measurement gives AVD close to the calculated average AVD. For a given cell voltage this leads to a few mm lower ACD, calculated from the measurements than ACD estimated by models. In spite of that, the models still have to be validated with measurements, because of unknown contact resistance in the stub-cast iron-carbon joints. This study demonstrates that the model calibration will be better if the modelled AVD to the measurement point is used instead of average AVD. It is also clear that a larger contact resistance in the cast iron – carbon joint should be used in the model for new anodes in comparison to mid-age and old anodes. As a refinement of the model, anode area reduction for mid-age and old anodes should be taken into account and the model sensitivity to greater curvature of the anode bottom surface should be tested; both may reduce the difference between the measured AVD and the average from the model.

Anode voltage drop is nearly the same for symmetric and asymmetric anodes, but the measured anode voltage drop is more overestimated in asymmetric anodes because of increased distance from stub to anode side at the back-wall.

Efforts to decrease ETJ voltage drop should be focused on the steel part because the aluminium part contributes very little to ETJ voltage drop.

## 11. References


1. Gennady V. Arkhipov, The mathematical modeling of aluminum reduction cells, *JOM,* Vol 56 Issue 2, February 2006, 54-55.
2. Amit Gupta et al., Investigation of cathode & collector bar modification on thermal balance of a low amperage cell. *Light metals* 2015*,* 747-752.
3. François Allard et al., The impact of the cavity on the top heat losses in aluminum electrolysis cells, *Light metals* 2016*,* 289-294.
4. Burkhard Sachs et al., 3D thermo-electric modelling of aluminium reduction cells including equilibrium ledge profile prediction, *Proc. of 35th International Conf. of ICSOBA*, Hamburg, Germany, 2-5 October 2017, Paper AL18, *Travaux* 46, 955-961.
5. Marc Dupuis and Imad Tabsh, Thermo-electric analysis of the Grande-Baie aluminum reduction cell, *Light Metals* 1994, 339-342.
6. Mohamed I. Hassan et al., Validation of Anode Model for Voltage Drop Mitigation Studies, *Proc. of 34th International Conf. of ICSOBA*, Quebec, Canada, 3-6 October 2016, Paper AL36, *Travaux* 45, 847-857.
7. Hicham Chaouki et al., Finite element analysis of slot size effect on the thermal-electrical behaviour of the anode, *Light Metals* 2017, 1315-1323.
8. Munir Baiteche et al., Hydrodynamic and thermoelectric 3D mathematical model of aluminium electrolysis cell to investigate slotted carbon anode efficiency, *Light Metals* 2017, 1323-1331.
9. Dagoberto Severo and Vanderlei Gusberti, Design options to reduce specific energy consumption in aluminium electrolysis cells. *Proc. of 34th International Conf. of ICSOBA,* Quebec, Canada, 3-6 October 2016, Paper Al04, *Travaux* 45, 505-517.
10. Warren E. Haupin, Interpreting the components of cell voltage, *Light Metals* 1998, 531-537.